Desalination and Water Treatment
www.deswater.com

doi: 10.5004/dwt.2023.29206

284 (2023) 194–204
February

A comprehensive study on the photocatalytic processes using N-doped $FeNi_3/TiO_2$ magnetic nanocomposite as a novel photocatalyst for removal of RR195 dye

Z. Sahebdadzehi[a], M. Khodadadi[b,*], H. Dorri[c]

[a]*Student Research Committee, Birjand University of Medical sciences, Birjand, Iran*
[b]*Department of Environmental Health Engineering, Birjand University of Medical sciences, Birjand, Iran, Tel. 05632381661; email: maryam.khodadadi@gmail.com*
[c]*Social Determinants of Health Research Center, Department of Environmental Health Engineering, Birjand University of Medical Sciences, Birjand, Iran*

Received 11 June 2022; Accepted 6 December 2022

ABSTRACT

The present paper aimed to synthesize and characterize N-doped $FeNi_3/TiO_2$ nanocomposite as well as its application to decompose Reactive Red 195 dye (RR195) from aqueous solutions. Characterization studies including Fourier-transform infrared spectroscopy, field-emission scanning electron microscopy, Brunauer–Emmett–Teller, and vibrating-sample magnetometer systems showed that N-doped $FeNi_3/TiO_2$ nanocomposite specifications containing morphology, magnetic properties, and formed functional groups were confirmed. The results of photocatalytic experiments showed that the degradation performance of RR195 dye under optimal conditions (pH = 3, photocatalyst dose 2 g/L, dye concentration = 20 mg/L, reaction time = 60 min) reached 96%, and chemical oxygen demand results approved the formation of intermediate compounds. Moreover, the results of the reusability study demonstrated that degradation percentage of RR195 decreased to 65% during 5 cycles. It can be concluded that N-doped $FeNi_3/TiO_2$ nanocomposite has a good potential and practical ability to eliminate RR195 from an aqueous medium.

Keywords: N-doped $FeNi_3/TiO_2$ synthesis; Reactive Red 195 dye; Photocatalytic reaction

1. Introduction

Currently, the world is facing great challenges in the fields of water management and environmental pollution by anthropogenic sources including industrial wastewater [1–3]. Generally, these fields require the continual seeking and developing of innovative and high-performance purification technologies for water and wastewater. In addition, the development of industries and the increasing pace of production in the last three decades have exacerbated the problems resulting from the pumping of industrial effluent-containing contaminants into water resources and environment [4–6]. In fact, insufficient or imperfect treating industrial wastewater can cause high concentrations of contaminants to enter the environment that it can eventually have adverse effects on the environment and human health [4,6,7]. For example, it was found that approximately 22% of the total quantity of used raw dyes is released with inadequately treated wastewater from various industries such as leather and tannery, textiles, cosmetics, food, printing and plastics industries [8,9].

* Corresponding author.

Estimates also show that about one-fifth of the total dye production in the textile industries is transferred to the environment through wastewater [9,10]. Dyes are divided into three main categories including anionic (direct, acidic and reactive), cationic (total primary dyes) and non-ionic (dispersed dyes) [10,11]. Azoic dyes are the largest group of dyes which is used for textile dyeing and other industrial applications. Most dyes cause adverse effects such as allergies, dermatitis, skin irritation, cancer and genetic mutations in humans in the long term if they enter the environment. These compounds also have an aesthetic negative effect on water quality [11–13]. Reactive dye 195 contains an active group consisting of an aromatic heterocyclic ring containing fluoride or chloride ions. This dye is commonly used for dyeing cellulose fabrics and fabric textures. The presence of these aromatic rings makes these compounds resistant to biodegradation and they can remain in the environment for a long time and then can lead to adverse effects on humans and the environment [12,14]. Therefore, these compounds must be eliminated and mineralized before entering the environment. One of the superior and efficient treatment methods that can be used to degrade various organic pollutants is advanced oxidation processes (AOP_S) [13]. In most cases, these remediation ways can decompose the hard or non-biodegradable organic matter by using active free radicals produced during oxidation reactions [15]. The photocatalytic process is among the most efficient and diversely applied ways for the degradation of organic matter such as dyes [12]. In these processes, the working mechanism generally produces active free radicals in the simultaneous presence of a light source (sunlight, simulated sunlight, and UV) and a semiconductor material (e.g., TiO_2 and ZnO). In this way, the collision of light with semiconductor material can lead to the excitation of an electron and its transfer from the gap band to the conduction band. Simultaneously, active cavities ($hole^+$; h^+) are formed at the photocatalyst surface [15–17]. Ultimately, the reactive radical hydroxyl (OH•) will be created during the reaction of water molecules or OH^- ions with h^+. Titanium dioxide nanoparticles are one of the most functional nanoparticles which are used as a catalyst in the photocatalytic process for the removal of organic matter [17,18]. Their advantages included non-toxic, high chemical stability in a wide range of pH, high performance in electron conduction as a semiconductor and etc. [15,17]. In the photocatalytic heterogeneous reaction, the retrieval of catalyst for reuse needs filtration or centrifuge processes. To overcome this problem, coating photocatalytic shells on magnetic compounds is one of the most feasible and easiest ways for recycling the catalyst [19,20]. $FeNi_3$ is an iron-nickel-based magnetic material that has recently been used in studies as a magnetic core because of the high saturation magnetism in its structure [21,22]. On the other hand, doping nanomaterials such as nitrogen (N), and carbon (C) on the photocatalytic shell reduces the electron–$hole^+$ (e^-–h^+) recombination property and improves the photocatalytic activity of a composite under visible light with a wavelength of more than 400 nm [23–25]. Therefore, this study aimed to synthesize and characterize N-doped $FeNi_3/TiO_2$ nanocomposite and its application to decompose Reactive Red 195 dye from aqueous solutions.

2. Materials and methods

2.1. Chemicals and apparatus

The dye used in present research was Reactive Red 195 dye (RR195) with a molecular weight of 1136.32 and molecular formula $C_{31}H_{19}ClN_7Na_5O_{19}S_6$ and the molecular structure of RR195 is depicted in Fig. 1. Other materials include hydrazine hydrate ($N_2H_4.H_2O$: 80% purity), ethanol (C_2H_5OH), titanium butoxide (TBOT: $Ti(OBu)_4$ (Bu = $CH_2CH_2CH_2CH_3$)), iron chloride ($FeCl_2.4H_2O$), hydrogen peroxide (H_2O_2; 30%), polyethylene glycol (1g MW 600), nickel chloride ($NiCL_2$; $6H_2O$), HCl, and NaOH were the product of Merck Company. In order to measure the residual dye concentration, a spectrophotometer (model: UV/Vis T80+) at a wavelength of 540 nm was used.

2.2. N-doped $FeNi_3/TiO_2$ composite synthesis method

2.2.1. Synthesis of Fe-Ni_3

First, 1 g of polyethylene glycol was dissolved in 180 mL of water. Next 0.713 g of nickel chloride and 0.198 g of iron chloride were separately dissolved in two containers containing 30 mL of distilled water and then added to the first suspension. After complete mixing, the pH of the suspension was adjusted between 12 and 13 by using sodium hydroxide. Then 1.9 mL of hydrazine hydrate was added to the previous suspension and the reaction was performed for 24 h. Simultaneously with the progress of the reaction, the solution pH was regularly monitored to maintain the desired range. Finally, the obtained product was washed several times with water and ethanol, and it was dried at 30°C in a vacuum oven after separation by an external magnetic field [22].

2.2.2. Synthesis of $FeNi_3/TiO_2$ nanocomposites

0.2 g of $FeNi_3$ was mixed in a mixture containing 10 mL of 1-propanol and 50 mL of distilled water. Next, 2 mL of TBOT (tetrabutyl orthotitanate) was added drop by drop to the previous suspension and stirred for 24 h at 500 rpm at 80°C. Next, the obtained $FeNi_3/TiO_2$ nanocomposite is washed with water and ethanol in several steps. This nanocomposite is dried in a vacuum oven at 30°C after separation by an external magnetic field. Ultimately, the samples are placed to calcine in a furnace at 400°C for 4 h [15].

2.2.3. Synthesis of N-doped $FeNi_3/TiO_2$ nanocomposites

First, 140 mg of $FeNi_3/TiO_2$ was dispersed in 70 mL of distilled water for 20 min by ultrasonic waves. Next, its pH

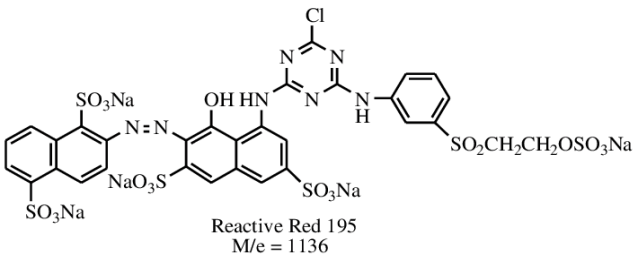

Fig. 1. Molecular structure of RR195.

was adjusted to 10 by ammonia 35%, and 2 mL of hydrazine hydrate was immediately added to it and shaken. The obtained suspension was heated in a Teflon autoclave for 80 h at 80°C. Ultimately, the formed particles were washed with distilled water and dried in a vacuum oven at 50°C. The schematic illustration of N-doped $FeNi_3/TiO_2$ synthesis is depicted in Fig. 2.

2.3. Characterization of $FeNi_3/TiO_2$ nanocomposite

To characterize $FeNi_3/TiO_2$ nanocomposite, Fourier-transform infrared spectroscopy (FT-IR) analysis (Model: Avatar 370, America), field-emission scanning electron microscopy (FE-SEM) image (Model: Zeiss-EM10C-100Kv, Germany), vibrating-sample magnetometer (VSM systems; Model Lake Shore 7404, America) and analyze of BET (Brunauer–Emmett–Teller; the BELSORP-MINI X sorption analyzer) were used.

2.4. Photocatalytic tests

The schematic of photocatalytic reactor is shown in Fig. 3. In this research to prepare samples, the stock solution of RR195 was made by dissolving 1 g of RR195 powder in 1,000 mL distilled water, and also to investigate the photocatalytic degradation of RR195 using N-doped $FeNi_3/TiO_2$ nanocomposite in the presence of UV irradiation, the impression of various parameters including pH (3, 5, 7, 9 and 11), the dose of N-doped $FeNi_3/TiO_2$ (0.055, 0.01, 0.02, 0.03, 0.04, 0.05 and 0.1 g/L) and initial concentration of RR195 (2, 5, 10 and 15 mg/L) at reaction times (5, 10, 15, 30, 60, 80, 120 and 180 min) was investigated. To supply the UV irradiation, a UV lamp was installed in the middle of the reactor with a power of 2,500 W/cm^2 and a wavelength of 254 nm. To consider the adsorption and desorption of RR195, the prepared solutions were put in the darkness for 0.5 h. At the end of each step of the test, the residual concentration of RR195 was determined by the spectrophotometry in the wavelength of 540 nm. It should be noted that since the maximum absorption of RR195 by nanoparticles synthesized in optimal conditions was 8%–12%, it was not discussed in the results of this research.

2.5. Kinetics study

In the photocatalytic process, reaction kinetics can be used to evaluate the degradation rate of pollutants by modeling its degradation. Pseudo-first kinetic models are used to express the speed of heterogeneous photocatalytic degradation of organic matter such as RR195. Langmuir–Hinshelwood kinetics model is broadly used to describe the reaction kinetics [Eq. (1)] [27].

$$r = k'\theta = -\frac{dc}{dt} = k'\left(\frac{KC}{1+KC}\right) \tag{1}$$

where K, k', r, θ and C are the uptake coefficient of reactant, the constant of reaction rate (1/min), the oxidation reaction rate (mg/L·min), the fractional site coverage for RR195 and RR195 concentration (mg/L), respectively. In the solutions with very low concentrations of contamination and $K \ll 1$, the Langmuir–Hinshelwood equation may be simple as Eqs. (2) and (3).

$$-\frac{dc}{dt} = K_{obs} \tag{2}$$

$$\ln\left(\frac{C}{C_0}\right) = -K_{obst} \tag{3}$$

where C_0, K_{obs}, t and C are primary concentration of RR195 (mg/L), constant of pseudo-first-order reaction rate (min^{-1}), reaction time (min) and RR195 concentration at time of t (mg/L).

2.6. Reusability study

Assessment stability and reusability of the photocatalysts is one of the important parameters that need to be

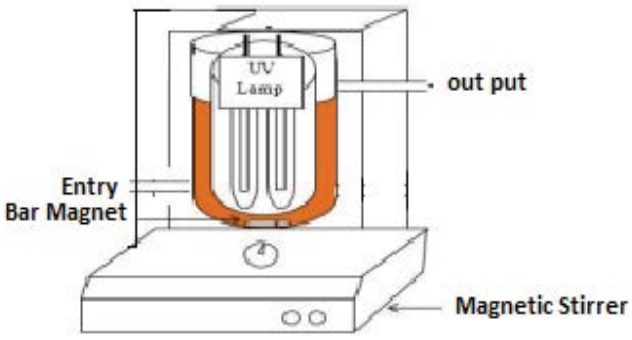

Fig. 3. Schematic of photo-catalytic reactor.

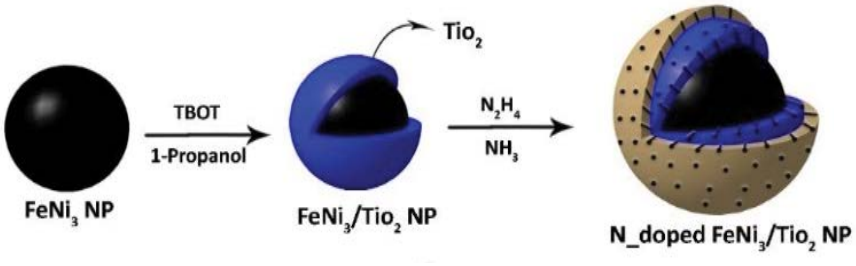

Fig. 2. Schematic illustration of N-doped Fe-Ni_3/TiO_2 synthesis.

studied. To survey it, the potential reuse of the N-doped $FeNi_3/TiO_2$ nanocomposite under UV light has been investigated to degrade RR195 dye during five times. After each reaction, the N-doped $FeNi_3/TiO_2$ nanocomposite was separated from the reactor by using a magnet and was washed repeatedly with distilled water, and then re-entered the reactor as a photocatalyst to degrade RR195 dye after drying at 80°C. Ultimately, the residual concentration of the dye was separately measured to evaluate the decrease in photocatalyst activity after each cycle.

2.7. Chemical oxygen demand experiment

Chemical oxygen demand (COD) test has been implemented according to standard 5310B protocol, taken from the standard manual for water and wastewater experiments. This test can indirectly confirm the presence or absence of potentially formed intermediates. Therefore, after obtaining the optimal conditions, a COD test was carried out [28].

3. Results and discussion

3.1. Characterization study

3.1.1. FT-IR spectroscopy

FT-IR spectroscopy was used to identify the functional groups of N-doped $FeNi_3/TiO_2$ magnetic nanocomposites and the results are depicted in Fig. 4. The tensile vibrations of Fe–Ni, Ni–Fe–Ni and, Fe–Ni–Ni bonds presence corresponded to a peak at 494 cm^{-1}. The presence of a peak in 1,347.73 cm^{-1} is related to the vibration of C–H and N–O bonds, which is occurred due to the residue of some raw materials such as hydrazine hydrate in the synthesis stages. The absorption band at 3,937.85 cm^{-1} is related to the vibrations of the hydroxyl functional group (O–H) in the sample, which may be due to the presence of moisture. The Ti–O–Ti bond is responsible for vibration at 792 and 1,102 cm^{-1}. The wide peak at 3,819 cm^{-1} is due to the tensile vibration caused by the O–H bond. On the other hand, vibrations in 1626, 675 and 590 cm^{-1} bands confirm the presence of the TiO_2 shell on the $FeNi_3$ magnetic core. The compact and wide bands between 1,078 and 964 cm^{-1} were attributed to the strong tensile vibrations of the Ti–O and Ti–O–Ti bonds, and it is indicated that the distance between the TiO_2 band and N-doping is decreased [29–34].

3.1.2. FE-SEM image

To study the shape, surface and average diameter of particles an electron microscope (FE-SEM) was used, and its results are shown in Fig 5. Fig. 5A and B both show the surface image of the synthesized nanocomposite, except that Fig. 5B examines the surface of nanoparticles with high-resolution. According to Fig. 5, it can be inferred that N-doped $FeNi_3/TiO_2$ particles have a property of aggregation, which is due to their magnetic properties that cause the particles to be well absorbed and placed next to each other. Due to their amorphous state and no deformation in different modes, a regular structure is not recommended for N-doped $FeNi_3/TiO_2$ nanocomposite. On the other hand, it can be seen that N-doped $FeNi_3/TiO_2$ nanocomposite has a rough surface. The average size of the N-doped $FeNi_3/TiO_2$ nanocomposite was determined between 33.5 and 67.31 nm, and its texture is compressibility dense, which indicated its high density.

3.1.3. VSM technique

To evaluate the magnetic properties of N-doped $FeNi_3/TiO_2$ nanocomposite, a VSM system was used at room

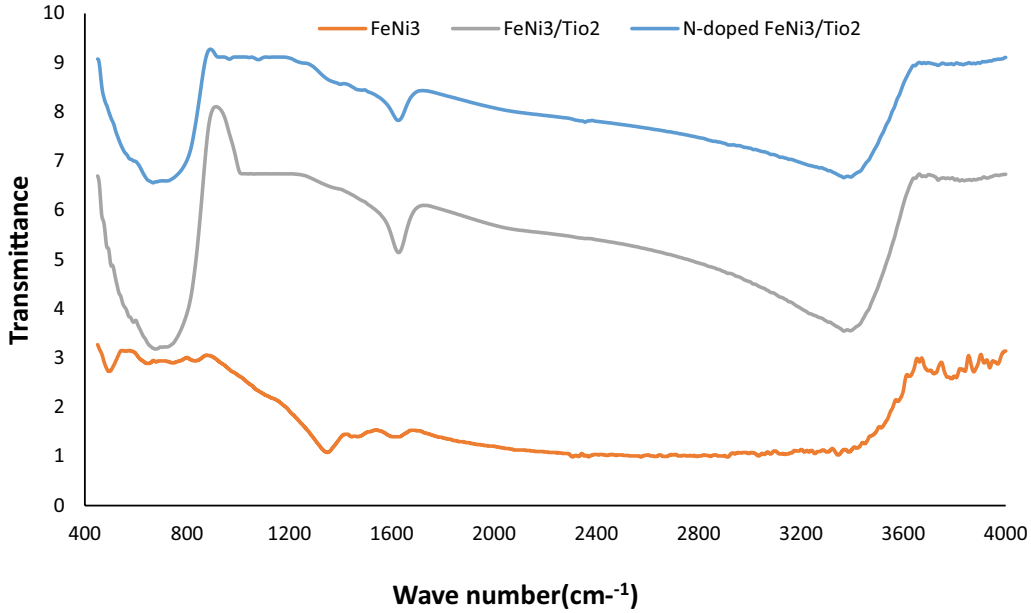

Fig. 4. FT-IR spectroscopy of N-doped $FeNi_3/TiO_2$.

temperature, and its result can be seen in Fig. 6. According to the results, $FeNi_3$, $FeNi_3/TiO_2$, and N-doped $FeNi_3/TiO_2$ nanocomposite have a saturation magnetization of 69, 6.7, and 10.5 emu/g, respectively. The saturation magnetism decreased due to coating with titanium oxide and nitrogen doping. Actually, the decrease in M_s values final nanocomposite compared to the uncoated $FeNi_3$ is due to the layer coated on the surface of particles and the increase in size. Despite the decrease in saturation magnetization, these particles could still be easily separated using a magnetic field.

3.1.4. BET analysis

BET analysis was utilized to measure the specific surface area (m^2/g) of N-doped $FeNi_3/TiO_2$ nanocomposite and its results are expressed in Table 1. BET analysis showed that the specific surface area of the nanocomposite was 112.42 m^2/g. The high surface area obtained for nanocomposites can play an effective role in photocatalytic activity and absorption of ultraviolet beams.

3.2. Effect of variables

3.2.1. Effect of pH

In photocatalytic reactions, the decomposition performance can be affected by different factors, especially pH. Because of amphoteric behavior of the most semiconductor particles, pH can alter the charge features of the

Table 1
BET analysis of N-doped $FeNi_3/TiO_2$ nanocomposite

Nanoparticle	Surface area (m^2/g)	Average pore diameter (nm)	Pore volume (cm^3/g)
N-doped $FeNi_3/TiO_2$	112.48	7.7477	0.2186

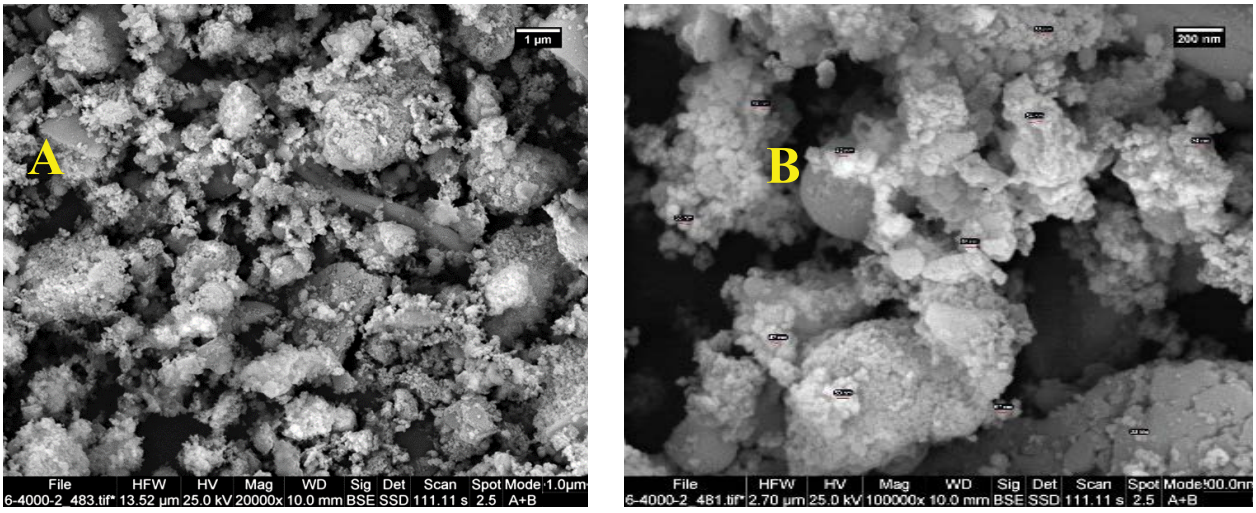

Fig. 5. FESEM image of N-doped $FeNi_3/TiO_2$ nanocomposite A (ordinary) and B (high resolution).

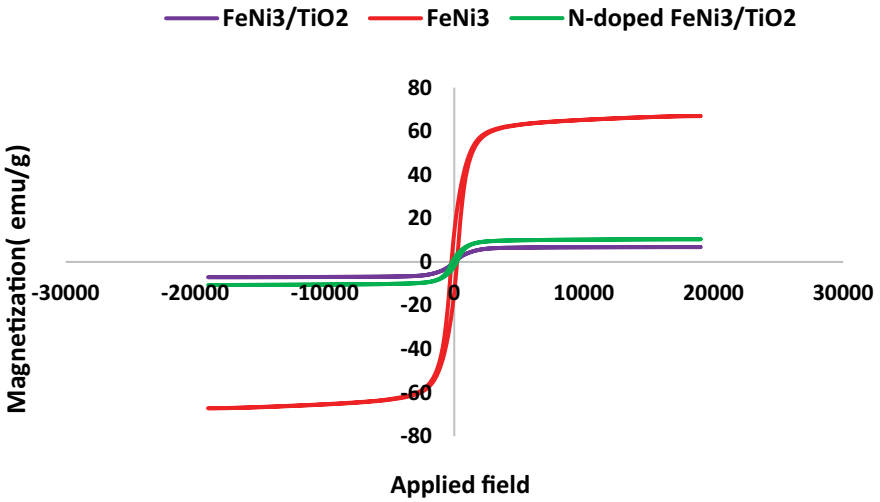

Fig. 6. VSM analysis of N-doped $FeNi_3/TiO_2$ nanocomposite.

photocatalyst surface. In other words, the effect of pH on the photocatalytic reaction is difficult because of electrostatic interplay between the catalyst surface, pollutant and free radicals formed during the reaction [35]. Therefore, before interpreting the effect of pH, we must clearly identify the possible contaminant and photocatalyst states at different pH. RR195 dye is an anionic compound meaning that its acidic constant (pKa) is in the acidic pH range, and therefore it will exist as a negative ion in relatively strong acidic and alkaline environments. Also, the photocatalyst surface charge is dependent on solution pH. Accordingly, the pH_{zpc} value of the photocatalyst was determined to specify the positivity and negativity charge of N-doped $FeNi_3/TiO_2$ nanocomposite. Based on the method used by Boumediene et al. [36], the pH_{zpc} value was measured and estimated to be close to 7.2. This means that at pH less than 7.2 the catalyst surface will have a positive charge and in contrast at pH more than 7.2 the catalyst surface will have a negative charge. To survey the effect of pH on RR195 degradation efficiency, it was adjusted between 3 and 11 and other effective factors (concentration RR195 = 20 mg/L, catalyst dose = 2 g/L, reaction time = 60 min) were constant. The obtained results are depicted in Fig. 7. Accordingly, maximum elimination percentage (98.8%) was achieved at pH = 3 (acidic condition), vs. minimum degradation percentage (71%) was observed in at pH = 11 (alkaline medium). In alkaline pH N-doped $FeNi_3/TiO_2$ nanocomposite surface and RR195 molecule are negatively charged, and the adsorption of RR195 on the photocatalyst surface decreased at alkaline pH. This repulsion factor prevents the contaminant from approaching the catalyst surface, and only dye removal agent in these conditions is suspended hydroxyl radicals ($OH^{\bullet}$) [37]. But in acidic conditions, in addition to hydroxyl, positive cavities can degrade the contaminants. In other words, in acidic conditions, due to the attraction between the contaminant and the photocatalyst surface, RR195 dye is simultaneously attacked by free radicals and positive holes, and the result is an increase in RR195 dye degradation efficiency. Similar results have been achieved in the studies conducted by other researchers, which is consistent with the findings of the present study [12,38].

3.2.2. Effect of N-doped $FeNi_3/TiO_2$ nanocomposite dose

Another important variable in the photocatalytic reaction is N-doped $FeNi_3/TiO_2$ nanocomposite dose catalyst. To evaluate the impact of the nanocomposite dose on the photocatalytic elimination of RR195, various values of N-doped $FeNi_3/TiO_2$ nanocomposite (1, 2, 4, and 6 g/L) under UV light have been investigated and its results are depicted in Fig. 8. It shows that the degradation efficiency of RR159 dye promotes by increasing the catalyst dose from 1 to 2 g/L but it was decreased following an increase in the catalyst dose. Increased efficiency at the beginning of the reaction can be due to the increase in the catalyst dose and the number of active sites at the photocatalytic surface [39]. Because the synthesized nanocomposites are magnetic, they can stick together at high concentrations, and form agglomeration particles that active sites on catalyst surface for UV absorption is consequently reduced [7,15,19]. Moreover, a further increase in the nanocomposite dose can lead to creating turbidity in the solution, and it ultimately reduces the degradation efficiency [40].

3.3. Effect of initial concentration

Initial concentration is another factor that affects the efficiency of the photocatalytic dye removal reaction using N-doped $FeNi_3/TiO_2$ nanocomposite. As shown in Fig. 9, the removal efficiency was decreased with increasing concentration of dye. At the lowest dye concentration, the removal percentage was 98.8% in reaction time equal 60 min and by increasing the dye concentration to 40 mg/L, the removal percentage was decreased to 58% in same time. The adsorbed contaminants on the nanocatalyst surface increase when the initial concentration increases, and it prevents direct contact of light with the catalyst,

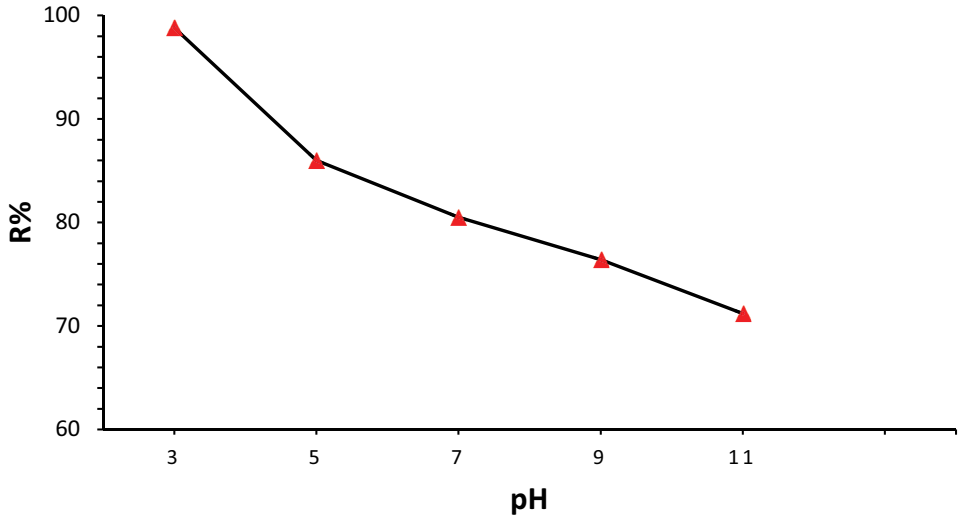

Fig. 7. Effect of pH on Reactive Red 195 dye removal by N-doped $FeNi_3/TiO_2$/UV light (concentration RR195 = 20 ppm; catalyst dose = 2 g/L; reaction time = 60 min).

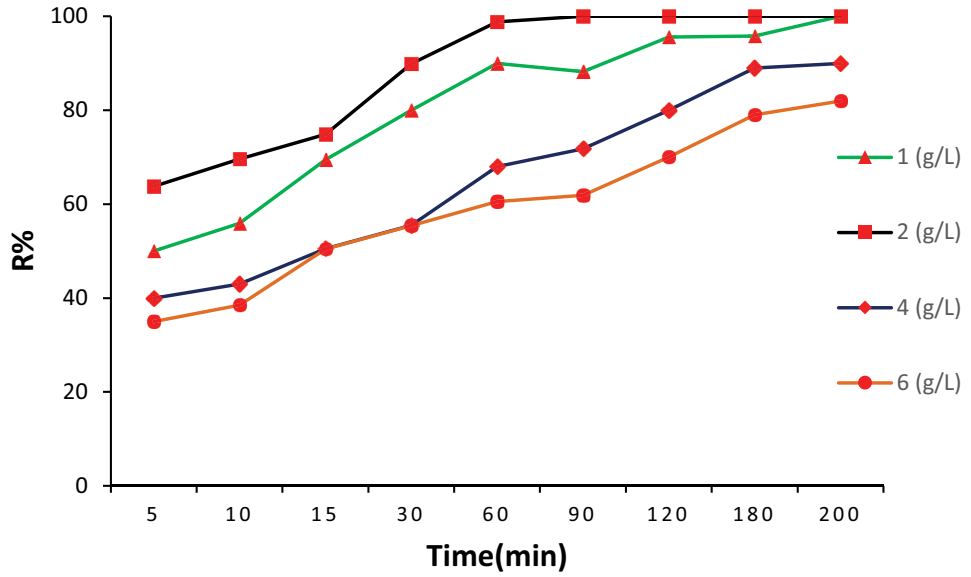

Fig. 8. Effect of nanocatalyst dose on efficiency of Reactive Red 195 dye removal by N-doped $FeNi_3/TiO_2$/UV light (pH = 3; concentration RR195 = 20 ppm).

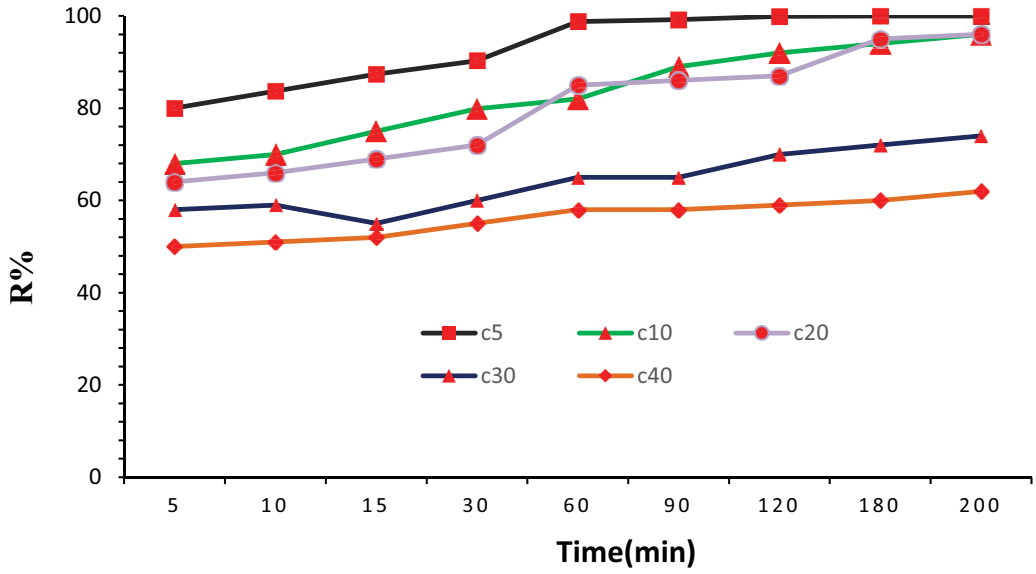

Fig. 9. Effect of initial concentration on efficiency of Reactive Red 195 dye removal by N-doped $FeNi_3/TiO_2$/UV light (pH = 3; catalyst dose = 2 g/L).

which is subsequently reduced the degradation efficiency of dye (40). In the study conducted by Khodadadi et al. [27], which is investigated the removal of tetracycline by the $FeNi_3/SiO_2/TiO_2$ photocatalyst, the results showed that increasing the concentration of the contaminant lead to reduce the degradation of tetracycline.

3.4. Kinetics study

First-order kinetics were used to investigate the kinetics of degradation reaction under the photocatalytic process, and the results are plotted in Fig. 10. The amount of K_{obs} (kinetic constants) at different concentrations and times shows that its value decreases with increasing color concentration. Based on studies conducted by researchers, it was found that the degradation constant rate of pollutants reduces when the concentration of pollutants is increasing. The cause of this phenomenon is that by increasing the concentration dye in the presence of constant catalyst value and free radical produced, the rate of pollutant decomposition descends. Furthermore, by-products created during the reaction can react with radicals and reduce dye decomposition [41–43]. On the other hand, the obtained K_{obs} along with the determination coefficient values (R^2) are expressed in Table 2. The determination coefficients show that K_{obs} values are obtained with high confidence.

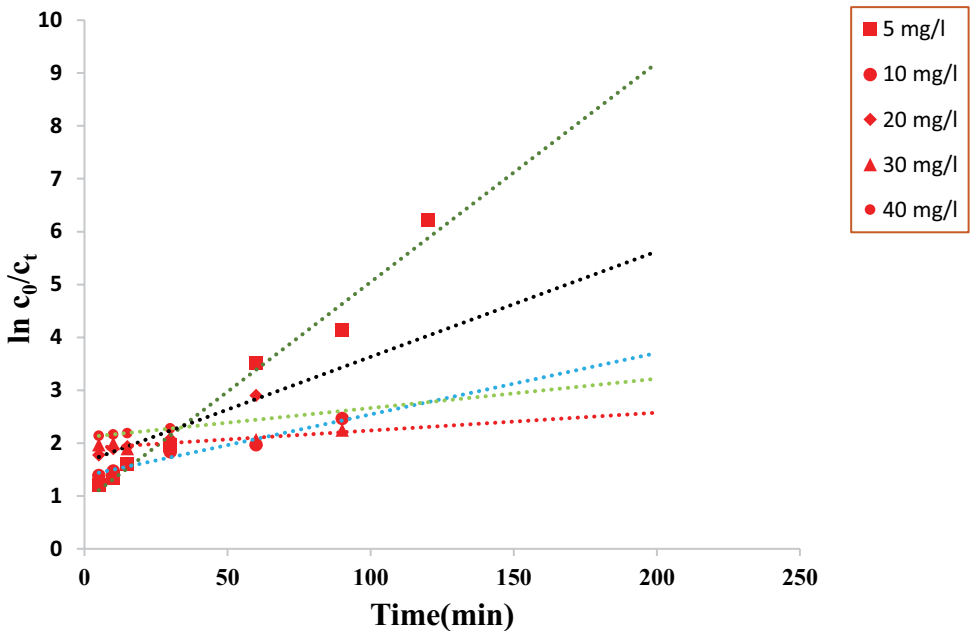

Fig. 10. Kinetics of reaction.

Table 2
Reaction kinetics and the relevant data

RR195 concentration (mg/L)	Equation	K_{obs} (min^{-1})	R^2	$t_{1/2}$ (min)
5	$y = 0.0415x + 0.9004$	0.0415	0.97	16.6988
10	$y = 0.0116x + 1.3816$	0.0116	0.96	59.74138
20	$y = 0.0199x + 1.6374$	0.0199	0.95	34.82412
30	$y = 0.0034x + 1.9009$	0.0034	0.81	203.8235
40	$y = 0.0055x + 2.1085$	0.0055	0.99	126

3.5. Degradation mechanism

The presence of semiconductor materials such as TiO_2 is one of the main features which is required for photocatalytic activity. The main trait of this material is the existence of conduction and gap bands in that structure. It can lead to the transition of electrons from the gap band to conduction by receiving energy from the emitted beam and simultaneously creating holes+ (h^+) in the photocatalyst surface. The created h^+ can decompose organic matter directly and it can indirectly react with water molecules or hydroxyl ions (OH) that lead to product hydroxyl radicals ($OH^\bullet$) that eliminate organic matter. Moreover, irritated electrons may react with O_2 and product radicals. In addition, hydrogen peroxide is formed during chain reactions that it can eventually produce $OH^\bullet$. Possible reactions in the photocatalytic reactor are described below. The formed $OH^\bullet$ by high redox potential attack the RR195 molecules and degrade it to water and carbon dioxide as well as possible by-products (easily biodegradable polymers). As shown in Fig. 11, the amount of residual dye and its COD in the photocatalytic process is significantly different due to the formation of possible intermediate compounds [12,15].

$$TiO_2 \xrightarrow{h\vartheta} TiO_2\left(e^- + h^+\right) \quad (4)$$

$$TiO_2\left(h^+\right) + H_2O \rightarrow OH^\bullet + H^+ + TiO_2 \quad (5)$$

$$TiO_2\left(h^+\right) + OH^- \rightarrow OH^\bullet + TiO_2 \quad (6)$$

$$TiO_2\left(e^-\right) + O_2 \rightarrow {}^\bullet O_2^- + TiO_2 \quad (7)$$

$$O_2^{\bullet-} + H_2O \rightarrow HO_2^\bullet + OH^- \quad (8)$$

$$2HO_2^\bullet \rightarrow H_2O_2 + O_2 \quad (9)$$

$$H_2O_2 + TiO_2\left(e^-\right) \rightarrow OH^- + OH^\bullet + TiO_2 \quad (10)$$

$$RX_{ads} + TiO_2\left(h^+\right) \rightarrow TiO_2 + RX_{ads}^{\bullet+} \quad (11)$$

3.6. COD removal in the photocatalytic oxidation process

The removal of COD in pH changes during the photocatalytic oxidation stage was investigated and according to Fig. 11, the highest efficiency of 40% was obtained at a pH equal to 3. The efficiency of COD removal decreases with the increase in the pH of the environment. The reason is the precipitation of iron in the form of hydroxide in an alkaline environment. Finally, the turbidity caused by deposition reduces the transmission of UV radiation [44–46].

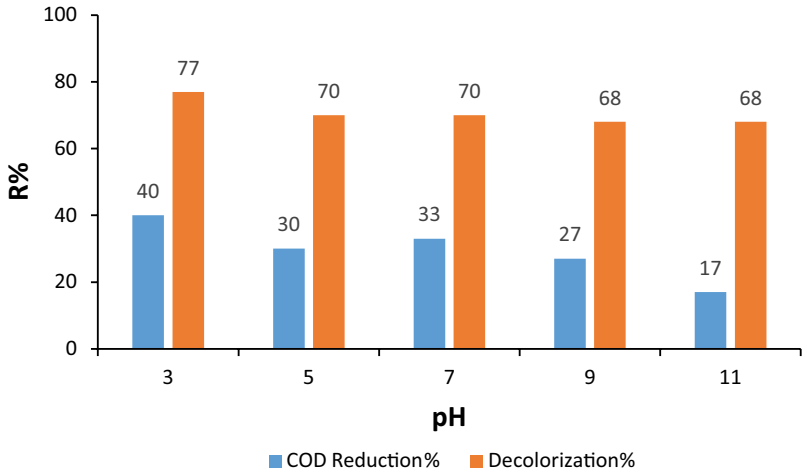

Fig. 11. COD removal in the photocatalytic oxidation process.

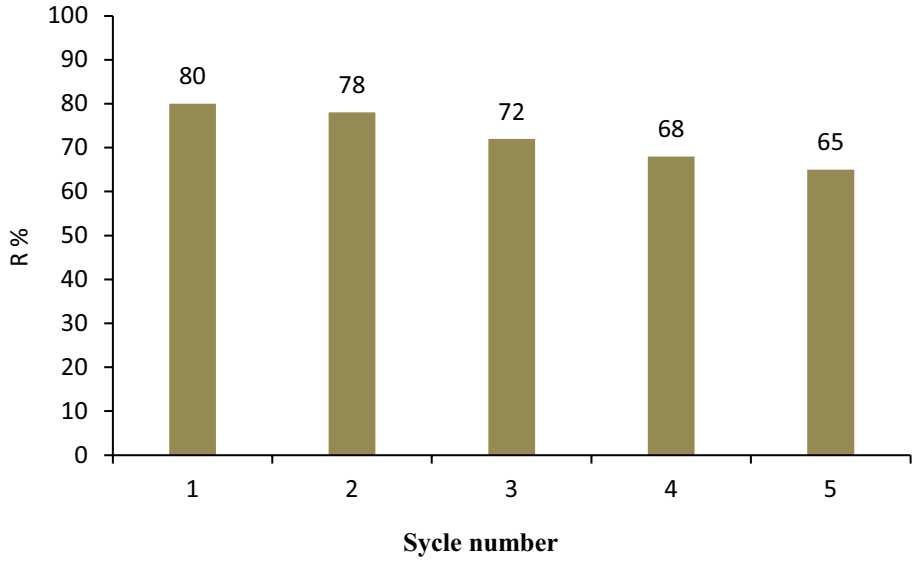

Fig. 12. Result of reusability study.

3.7. Reusability result

The results of the reusability study are depicted in Fig. 12. It indicates that a 35% reduction of catalyst has been seen during the photocatalytic activity after five times nanocomposite utility, and then the reusability percentage practically is acceptable.

4. Conclusion

The aim of this study was the synthesis and characterization of N-doped $FeNi_3/TiO_2$ nanocomposite as well as its application to decompose Reactive Red 195 dye from aqueous solutions. The results of the characterization study indicated that N-doped $FeNi_3/TiO_2$ nanocomposite specifications including magnetic properties, morphology, and formed functional groups in the structure were confirmed. The results of photocatalytic tests displayed that the degradation performance of RR195 dye in pH = 3, photocatalyst dose 2 g/L, dye concentration = 20 mg/L, reaction time = 60 min reached 96% and COD results confirmed the formation of by-product compounds. The results of reusability study represented that the degradation percentage of RR195 was reduced about 35% during 5 cycles. As a total result, it can say that N-doped $FeNi_3/TiO_2$ nanocomposite has a good potential and ability to decompose RR195 from aqueous solutions.

Acknowledgments

The authors gratefully acknowledge the support of this work by Birjand University of Medical Sciences.

References

[1] A. Hossein Panahi, A. Meshkinian, S.D. Ashrafi, M. Khan, A. Naghizadeh, G. Abi, H. Kamani, Survey of sono-activated persulfate process for treatment of real dairy wastewater, Int. J. Environ. Sci. Technol., 17 (2020) 93–98.

[2] E. Norabadi, A.H. Panahi, R. Ghanbari, A. Meshkinian, H. Kamani, S.D. Ashrafi, Optimizing the parameters of amoxicillin removal in a photocatalysis/ozonation process using Box–Behnken response surface methodology, Desal. Water Treat., 192 (2020) 234–240.
[3] N. Nasseh, M.T. Samadi, M. Ghadirian, A.H. Panahi, A. Rezaie, Photocatalytic degradation of tamoxifen by using a novel synthesized magnetic nanocomposite of $FeCl_2$@ac@ZnO: a study on the pathway, modeling, and sensitivity analysis using artificial neural network (AAN), J. Environ. Chem. Eng., 10 (2022) 107450, doi: 10.1016/j.jece.2022.107450.
[4] Y.F. Ting, S.M. Praveena, Sources, mechanisms, and fate of steroid estrogens in wastewater treatment plants: a mini review, Environ. Monit. Assess., 189 (2017) 1–19.
[5] D.A. Yaseen, M. Scholz, Treatment of synthetic textile wastewater containing dye mixtures with microcosms, Environ. Sci. Pollut. Res., 25 (2018) 1980–1997.
[6] V.S. Ashtekar, V.M. Bhandari, S.R. Shirsath, P.L.V.N. Sai Chandra, P.D. Jolhe, S.A. Ghodke, Dye wastewater treatment: removal of reactive dyes using inorganic and organic coagulants, J. Ind. Pollut. Control., 30 (2014) 33–42.
[7] N. Nasseh, B. Barikbin, L. Taghavi, Photocatalytic degradation of tetracycline hydrochloride by $FeNi_3/SiO_2$/CuS magnetic nanocomposite under simulated solar irradiation: efficiency, stability, kinetic and pathway study, Environ. Technol. Innovation, 20 (2020) 101035, doi: 10.1016/j.eti.2020.101035.
[8] R. Kishor, D. Purchase, G.D. Saratale, R.G. Saratale, L.F.R. Ferreira, M. Bilal, R. Chandra, R.N. Bharagava, Ecotoxicological and health concerns of persistent coloring pollutants of textile industry wastewater and treatment approaches for environmental safety, J. Environ. Chem. Eng., 9 (2021) 105012, doi: 10.1016/j.jece.2020.105012.
[9] P. Sharma, S.P. Singh, Pollutants characterization and toxicity assessment of pulp and paper industry sludge for safe environmental disposal, I. Haq, A.S. Kalamdhad, Eds., Emerging Treatment Technologies for Waste Management, Springer, Singapore, 2021, pp. 207–223.
[10] R. Kishor, D. Purchase, F. LFR, S.I. Mulla, M. Bilal, R.N. Bharagava, Environmental and health hazards of textile industry wastewater pollutants and its treatment approaches, (2020).
[11] D. Dadi, T. Stellmacher, F. Senbeta, S. Van Passel, H. Azadi, Environmental and health impacts of effluents from textile industries in Ethiopia: the case of Gelan and Dukem, Oromia Regional State, Environ. Monit. Assess., 189 (2017) 1–30.
[12] S.M. Rahimi, A.H. Panahi, N.S.M. Moghaddam, E. Allahyari, N. Nasseh, Breaking down of low-biodegradation Acid Red 206 dye using bentonite/Fe_3O_4/ZnO magnetic nanocomposite as a novel photo-catalyst in presence of UV light, Chem. Phys. Lett., 794 (2022) 139480, doi: 10.1016/j.cplett.2022.139480.
[13] F.S. Arghavan, A. Hossein Panahi, N. Nasseh, M. Ghadirian, Adsorption-photocatalytic processes for removal of penta-chlorophenol contaminant using $FeNi_3/SiO_2$/ZnO magnetic nanocomposite under simulated solar light irradiation, Environ. Sci. Pollut. Res., 28 (2021) 7462–7475.
[14] S. Song, J. Fan, Z. He, L. Zhan, Z. Liu, J. Chen, X. Xu, Electrochemical degradation of azo dye C.I. Reactive Red 195 by anodic oxidation on Ti/SnO_2–Sb/PbO_2 electrodes, Electrochim. Acta, 55 (2010) 3606–3613.
[15] M. Khodadadi, T.J. Al-Musawi, H. Kamani, M.F. Silva, A.H. Panahi, The practical utility of the synthesis $FeNi_3$@SiO_2@TiO_2 magnetic nanoparticles as an efficient photocatalyst for the humic acid degradation, Chemosphere, 239 (2020) 124723, doi: 10.1016/j.chemosphere.2019.124723.
[16] E. Bazrafshan, T.J. Al-Musawi, M.F. Silva, A.H. Panahi, M. Havangi, F.K. Mostafapur, Photocatalytic degradation of catechol using ZnO nanoparticles as catalyst: optimizing the experimental parameters using the Box–Behnken statistical methodology and kinetic studies, Microchem. J., 147 (2019) 643–653.
[17] A. Jahantiq, R. Ghanbari, A. Hossein Panahi, S.D. Ashraf, AD. Khatibi, Photocatalytic degradation of 2,4,6-trichlorophenol in aqueous solutions using synthesized Fe-doped TiO_2 nanoparticles via response surface methodology, Desal. Water Treat., 183 (2020) 366–373.
[18] U.G. Akpan, B.H. Hameed, Parameters affecting the photocatalytic degradation of dyes using TiO_2-based photocatalysts: a review, J. Hazard. Mater., 170 (2009) 520–529.
[19] M.S. Lucas, P.B. Tavares, J.A. Peres, J.L. Faria, M. Rocha, C. Pereira, C. Freire, Photocatalytic degradation of Reactive Black 5 with TiO_2-coated magnetic nanoparticles, Catal. Today, 209 (2013) 116–121.
[20] R. Chalasani, S. Vasudevan, Cyclodextrin-functionalized Fe_3O_4@TiO_2: reusable, magnetic nanoparticles for photocatalytic degradation of endocrine-disrupting chemicals in water supplies, ACS Nano, 7 (2013) 4093–4104.
[21] F. Akbari, M. Khodadadi, T.J. Al-Musawi, I.F. Varouqa, A. Naghizadeh, Degradation of humic acid using a solar light-photocatalytic process with a $FeNi_3/SiO_2/TiO_2$ magnetic nanocomposite as the catalyst, Desal. Water Treat., 241 (2021) 135–145.
[22] A. Hossein Panahi, M. Kamranifar, M.H. Moslehi, S. Rodriguez-Couto, N. Nasseh, Synthesis and characterization of $FeNi_3$ nanoparticles and their application as catalysts for penicillin G degradation in a Fenton-like reaction, Desal. Water Treat., 181 (2020) 391–398.
[23] J. Wang, Q. Li, J. Ren, A. Zhang, Q. Zhang, B. Zhang, Synthesis of bowknot-like N-doped Co@C magnetic nanoparticles constituted by acicular structural units for excellent microwave absorption, Carbon, 181 (2021) 28–39.
[24] J. Jiao, W. Qiu, J. Tang, L. Chen, L. Jing, Synthesis of well-defined Fe_3O_4 nanorods/N-doped graphene for lithium-ion batteries, Nanoresearch, 9 (2016) 1256–1266.
[25] Q. Sun, X. Zhang, R. Liu, S. Shen, F. Wu, A. Xie, Nickel-assisted synthesis of magnetic bamboo-shaped N-doped carbon nanostructure for excellent microwaves absorption, Synth. Met., 272 (2021) 116644, doi: 10.1016/j.synthmet.2020.116644.
[26] T.A. Vu, G.H. Le, H.T. Vu, K.T. Nguyen, T.T.T. Quan, Q.K. Nguyen, H.T.K. Tran, P.T. Dang, L.D. Vu, G.D. Lee, Highly photocatalytic activity of novel Fe-MIL-88B/GO nanocomposite in the degradation of reactive dye from aqueous solution, Mater. Res. Express, 4 (2017) 035038, doi:10.1088/2053-1591/aa6079.
[27] M. Khodadadi, M. Ehrampoush, M. Ghaneian, A. Allahresani, A. Mahvi, Synthesis and characterizations of $FeNi_3$@SiO_2@TiO_2 nanocomposite and its application in photocatalytic degradation of tetracycline in simulated wastewater, J. Mol. Liq., 255 (2018) 224–232.
[28] A. Altamirano Briones, I. Cóndor Guevara, D. Mena, I. Espinoza, C. Sandoval-Pauker, L. Ramos Guerrero, P. Vargas Jentzsch, F. Muñoz Bisesti, Degradation of meropenem by heterogeneous photocatalysis using TiO_2/fiberglass substrates, Catalysts, 10 (2020) 344, doi: 10.3390/catal10030344.
[29] F.S. Arghavan, T.J. Al-Musawi, E. Allahyari, M.H. Moslehi, N. Nasseh, A.H. Panahi, Complete degradation of tamoxifen using $FeNi_3$@SiO_2@ZnO as a photocatalyst with UV light irradiation: a study on the degradation process and sensitivity analysis using ANN tool, Mater. Sci. Semicond. Process., 128 (2021) 105725, doi: 10.1016/j.mssp.2021.105725.
[30] N. Nasseh, L. Taghavi, B. Barikbin, M.A. Nasseri, A. Allahresani, $FeNi_3/SiO_2$ magnetic nanocomposite as an efficient and recyclable heterogeneous Fenton-like catalyst for the oxidation of metronidazole in neutral environments: adsorption and degradation studies, Composites Part B, 166 (2019) 328–340.
[31] A. León, P. Reuquen, C. Garín, R. Segura, P. Vargas, P. Zapata, P.A. Orihuela, FT-IR and Raman characterization of TiO_2 nanoparticles coated with polyethylene glycol as carrier for 2-methoxyestradiol, Appl. Sci., 7 (2017) 49, doi: 10.3390/app7010049.
[32] H. Rongan, L. Haijuan, L. Huimin, X. Difa, Z. Liuyang, S-scheme photocatalyst Bi_2O_3/TiO_2 nanofiber with improved photocatalytic performance, Mater. Sci. Technol., 52 (2020) 145–151.
[33] L. Zhu, X. Kong, C. Yang, B. Ren, Q. Tang, Fabrication and characterization of the magnetic separation photocatalyst C-TiO_2@Fe_3O_4/AC with enhanced photocatalytic performance

under visible light irradiation, J. Hazard. Mater., 381 (2020) 120910, doi: 10.1016/j.jhazmat.2019.120910.
[34] Y. Huang, Z. Guo, H. Liu, S. Zhang, P. Wang, J. Lu, Y. Tong, Heterojunction architecture of N-doped WO_3 nanobundles with Ce_2S_3 nanodots hybridized on a carbon textile enables a highly efficient flexible photocatalyst, Adv. Funct. Mater., 29 (2019) 1903490, doi: 10.1002/adfm.201903490.
[35] M. Esmati, A. Allahresani, A. Naghizadeh, Synthesis and characterization of graphitic carbon nitride/mesoporous nano-silica (g-C_3N_4/KCC-1) nanocomposite as a novel highly efficient and recyclable photocatalyst for degradation of antibiotic in aqueous solution, Res. Chem. Intermed., 47 (2021) 1447–1469.
[36] M. Boumediene, H. Benaïssa, B. George, S. Molina, A. Merlin, Effects of pH and ionic strength on methylene blue removal from synthetic aqueous solutions by sorption onto orange peel and desorption study, J. Mater. Environ. Sci., 9 (2018) 1700–1711.
[37] A. Akbari, Z. Sabouri, H.A. Hosseini, A. Hashemzadeh, M. Khatami, M. Darroudi, Effect of nickel oxide nanoparticles as a photocatalyst in dyes degradation and evaluation of effective parameters in their removal from aqueous environments, Inorg. Chem. Commun., 115 (2020) 107867, doi: 10.1016/j.inoche.2020.107867.
[38] N. Tzikalos, V. Belessi, D. Lambropoulou, Photocatalytic degradation of Reactive Red 195 using anatase/brookite TiO_2 mesoporous nanoparticles: optimization using response surface methodology (RSM) and kinetics studies, Environ. Sci. Pollut. Res., 20 (2013) 2305–2320.
[39] K. Qin, Q. Zhao, H. Yu, X. Xia, J. Li, S. He, L. Wei, T.An, A review of bismuth-based photocatalysts for antibiotic degradation: insight into the photocatalytic degradation performance, pathways and relevant mechanisms, Environ. Res., 199 (2019) 111360, doi: 10.1016/j.envres.2021.111360.
[40] P.K. Boruah, S. Szunerits, R. Boukherroub, M.R. Das, Magnetic Fe_3O_4@V_2O_5/rGO nanocomposite as a recyclable photocatalyst for dye molecules degradation under direct sunlight irradiation, Chemosphere, 191 (2018) 503–513.
[41] S. Taghavi Fardood, F. Moradnia, A. Ramazani, Green synthesis and characterisation of $ZnMn_2O_4$ nanoparticles for photocatalytic degradation of Congo red dye and kinetic study, Micro Nano Lett., 14 (2019) 986–991.
[42] D. Tekin, H. Kiziltas, H. Ungan, Kinetic evaluation of ZnO/TiO_2 thin film photocatalyst in photocatalytic degradation of Orange G, J. Mol. Liq., 306 (2020) 112905, doi: 10.1016/j.molliq.2020.112905.
[43] N. Ali, A. Said, F. Ali, F. Raziq, Z. Ali, M. Bilal, L. Reinert, T. Begum, H.M.N. Iqbal, Photocatalytic degradation of Congo red dye from aqueous environment using cobalt ferrite nanostructures: development, characterization, and photocatalytic performance, Water Air Soil Pollut., 231 (2020) 1–16.
[44] V. Mahendran, P.R. Gogate, Degradation of Acid Scarlet 3R dye using oxidation strategies involving photocatalysis based on Fe doped TiO_2 photocatalyst, ultrasound and hydrogen peroxide, Sep. Purif. Technol., 274 (2021) 119011, doi: 10.1016/j.seppur.2021.119011.
[45] B. Khaled, Z. Nassira, H. Imene, Eco-friendly synthesis of self-regenerative low-cost biosorbent by the incorporation of CuO: a photocatalyst sensitive to visible light irradiation for azo dye removal, Environ. Sci. Pollut. Res., 27 (2020) 31074–31091.
[46] Y. Fahoul, K. Tanji, M. Zouheir, I. El Mrabet, Y. Naciri, A. Hsini, L. Nahali, A. Kherbeche, Novel River Sediment@ZnO–Co nanocomposite for photocatalytic degradation and COD reduction of crystal violet under visible light, J. Mol. Struct., 1253 (2022) 132298, doi: 10.1016/j.molstruc.2021.132298.